RSC Advances

ROYAL SOCIETY OF CHEMISTRY

www.rsc.org/advances

Puncture characterization of multilayered polypropylene homopolymer / ethylene 1-octene copolymer sheets

Guansong He[a,b], Fengshun Zhang[a,b], Huaning Yu[a], Jiang Li[a]*, Shaoyun Guo[a]*

[a] *The State Key Laboratory of Polymer Materials Engineering, Polymer Research Institute of Sichuan University, Chengdu 610065, China*

[b] *Institute of Chemical Materials, China Academy of Engineering Physics, Mianyang, Sichuan 621900, China*

ABSTRACT

This paper presented the studies of the puncture resistances of the conventional blend and multilayered structure sheets. The polypropylene homopolymer (HPP) / ethylene 1-octene copolymer (POE) alternating multilayered sheets were prepared though multilayered coextrusion. Polarized optical microscope (POM) photographs revealed that HPP and POE layers aligned alternately vertical to the interfaces and continuously parallel to the extrusion direction, indicating a better laminate structure. Puncture results demonstrated the conventional blend was less puncture-resistant than the multilayered samples. Obvious interfacial delamination occurred in the multilayered structure during the crack propagation, causing the puncture behavior developed into a staged rupture behavior. Hence the puncture resistance was enhanced by the special energy absorbing mechanisms including the plastic deforming independently, interfacial delamination and ductile tearing of the layers.

Keywords: Multilayered coextrusion; Puncture test; Delamination; Mechanism

* To whom correspondence should be addressed. (Prof. Li, Email: li_jiang@scu.edu.cn, Fax: 86-028-85466077)
* To whom correspondence should be addressed. (Prof. Guo, Email: nic7702@scu.edu.cn, Fax: 86-28-85405135)

1. Introduction

Puncture resistance is an important mechanical property in flexible materials, such as packaging films, protective gloves, etc. To understand the intrinsic puncture parameters is very important in the design and manufacture of the puncture resistant materials [1, 2]. However, compared with the conventional mechanical properties, such as tensile property, impact fracture, flexural behavior and tear property, the puncture resistance has gained little attention recently. Moreover, the reported investigations are either qualitative, and do not provide a fundamental understanding of the puncture mechanisms, or are not applicable to the materials with plastic deformation [3]. The next section outlines the reported works on puncture involving different behaviors of various materials.

Through the studies of the puncture resistance of protective gloves to surgical needle, 19 commercially available surgical glove liners were qualitatively ranked according to a measurement of the puncture force, in order to compare these materials in terms of puncture protection with respect to the single latex glove [4]. However, the thickness was not taken into account, and the results were only qualitative for purpose of comparison. The energy required to perforate the plaque and the peak load recorded in the puncture tests were used to characterize puncture performance of rigid plaques such as polycarbonates [5]. The maximum load was found to vary linearly with both the plunger diameter and the sample thickness, but no quantitative analysis of the results was performed. The quantitative characterization of puncture resistance has also been developed for geo-textiles and geo-membranes. A correlation was found between the puncture force and the tensile strength for the probes greater than 20 mm in diameter [6, 7]. However, according to the calculated results of elastomer membranes with large

deformations in the absence of friction using the Mooney strain-energy function, the puncture strengths were found to be much lower than their tensile and biaxial strengths [8], The maximum puncture force was proportional to the sheet thickness and the probe diameter. Moreover, the puncture of rubber membranes was controlled by a maximum local deformation that is independent of the probe geometry [3]. However, the results were only applicable in the case of elastic deformation. For the plastics those could undergo a certain degree of plastic deformation before the fracture, the puncture behavior would be much different. The observation of the damage zone around the perforated area of polyolefin showed that the obvious shear yielding could occur and had been demonstrated be the dominant toughening mechanism in this material during the perforation test [9].

Recently, the multilayered products have been increasing their presence in the plastic business, mainly for the synergistic combination of the physical properties of their individual layers [10-12]. And many literatures have shown that the layered structure had a better mechanical property [13-16]. However, the puncture resistance evaluation of multilayer materials is relatively rare. While the puncture failure of mono-material films can be described in a relatively straightforward manner and understood in terms of basic material behavior such as “brittle” or “ductile”, the situation for multilayered products composed of different types of materials is more complex. The puncture resistance of a multilayered laminate cannot be directly calculated from the properties of the constituents, *e.g.* through a “rule-of-mixtures” or similar approach. Lange [17] presented the puncture behaviors of some multi-layer packaging laminates composed of polymer/metal/paper. It was found that the puncture resistance depended on the perforation direction. Whereas the multi-layer laminates used had only up to four layers,

and the components were not entirely composed of polymers. Thus it could not give an effective feedback to the research of puncture resistance evaluation of multilayered polyolefin obtained by continuous on-line processing.

In this work, the multilayered polypropylene-ethylene homopolymer / ethylene 1-octene copolymer (HPP/POE) sheets with alternating HPP and POE layers were prepared by multilayered coextrusion technology that was developed in our lab. Then, the effects of phase structure, layer number and the volume fraction of POE on the puncture resistance were examined.

2. Experimental section

2.1 Materials

The HPP used in this work was T38F from Lanzhou Petrochemical Company (China) with a melt flow rate (measured at 230˚C and 2.16 kg) of 3.0 g/10 min. The POE was Engage 8150 from Dupont-Dow Chemical consisting of 25 wt% octane, with a melt flow rate (measured at 190˚C and 2.16 kg) of 0.5 g/10 min. In addition, the shear moduli of HPP and POE were 1065 MPa and 30 MPa, respectively.

2.2 Samples preparation

Multilayered sheets consisted of alternating HPP and POE layers were extruded through the multilayered coextrusion system designed in our lab [18-21]. The 2-, 8-, 16-, 32-, 64- and 128-layer specimens were extruded by varying the number of LMEs. By varying the extruder screw speed ratios, the samples containing different POE volume fractions were obtained. For each multilayered sheet, totally three kinds of POE volume fractions were extruded through adjusting the extruder screw speed ratios of HPP and POE as 8:2, 7:3 and 6:4, respectively. In addition, the neat HPP sheet was also fabricated by one single-screw extruder (SJ-30) without the layer multiplying element

(LME). The temperature profile was in the range of 140-190˚C for HPP and POE. The temperatures of LME and coextrusion block were both 190˚C. For comparison, the conventional blended HPP/POE specimens were also extruded as sheets with the same dimension. The blends with the same volume fraction of POE as that in 2-layer structure were firstly mixed in a high-speed mixer, and then extruded using an extruder of multilayered coextrusion system in order to keep the same history as corresponding multilayered sheets. The thickness of each film sheet was approximately 1.5 mm after going through the fixed gap of the water cooling roll.

2.3 Density Measurement

The densities of multilayered composites were tested by a GH-120M high precision density tester (Matsuhaku, Taiwan), the measuring accuracy of which was 0.0001g/cm^3.The measured densities of the HPP and POE were 0.8986×10^3 and 0.8362×10^3 kg/m^3, respectively. According to the measured density of the composite, ρ_C, the volume fraction of the POE (V_{POE}) could be determined by the following equation:

$$V_{POE} = \frac{\rho_C - \rho_{HPP}}{\rho_{POE} - \rho_{HPP}} \quad (1)$$

where, ρ_C is the density of the composite, ρ_{POE} and ρ_{HPP} represent the densities of the POE and HPP, respectively. The sample codes and their volume fraction of POE were listed in Table 1.

Table 1 The content of the POE in the multilayered and blend samples

Sample Code		Average layer thickness (μm)		Density (g/cm^3)	Volume fraction of POE (%)
		HPP	POE		
Blend	6:4	–	–	0.8759	36.36%
	7:3	–	–	0.8862	19.80%
	8:2	–	–	0.8911	12.08%
2L	6:4	954.6	545.4	0.8759	36.36%
	7:3	1211.0	299.0	0.8862	19.80%
	8:2	1323.2	181.8	0.8911	12.08%
8L	6:4	227.1	147.9	0.8740	39.43%
	7:3	296.2	80.0	0.8853	21.27%
	8:2	322.5	55.0	0.8895	14.56%
16L	6:4	118.2	69.7	0.8746	38.42%
	7:3	148.0	39.5	0.8854	21.09%
	8:2	162.1	26.0	0.8901	13.81%
32L	6:4	57.3	36.4	0.8744	38.86%
	7:3	73.2	20.6	0.8849	22.01%
	8:2	80.1	13.9	0.8894	14.79%
64L	6:4	27.4	19.5	0.8727	41.51%
	7:3	35.8	11.3	0.8837	23.93%
	8:2	39.2	7.9	0.8881	16.82%
128L	6:4	14.2	9.3	0.8740	39.48%
	7:3	17.9	5.6	0.8838	23.71%
	8:2	19.9	3.7	0.8888	15.66%

2.4 Puncture test

The puncture tests were performed on an Instron5567 tension machine (Canton, MA, USA) with a 1000 N load cell at a room temperature of 23˚C. Before being placed in a circular holder with a diameter of 30 mm, the sample was cut into the circular form with a diameter slightly smaller than that of the holder. The probe fastened on the puncture device was lowered as close as possible to the film specimen, without making contact, before the test was started. The test set-up is depicted in Fig. 1. Three different probes with diameters of 1, 2 and 4 mm, respectively, were employed. The diameter and shape

of probe tip could affect the puncture behaviors. Das[22, 23] found in contrast to a rigid, flat bottom punch and a punch with sharp tip, for these needles, puncturing of the gel does not occur continuously but intermittently with the fracture progressing alternately in the wedge opening and the shear fracture modes. And a co-operative effect could be found for Puncturing of soft gels with multi-tip needles. Here, all puncture heads were hemispherical designed. As proved, the results obtained with the hemispherical probe can give the highest reproducibility [17]. The tests were conducted with a crosshead speed of 50 mm/min. The force and the displacement were measured and recorded. It should be noted that puncture strength was considered to be calculated as follows:

$$P_S = \frac{F}{d} \tag{2}$$

where P_s is the puncture strength (kN/m), and F is the maximum force (N), and d is the specimen thickness (mm). In addition, the energy that was absorbed until failure, expressed as puncture energy, was calculated by the computer integration of the load-displacement curves. The multilayered specimens were all perforated from the HPP layer to the POE layer. Each test was repeated at least five times.

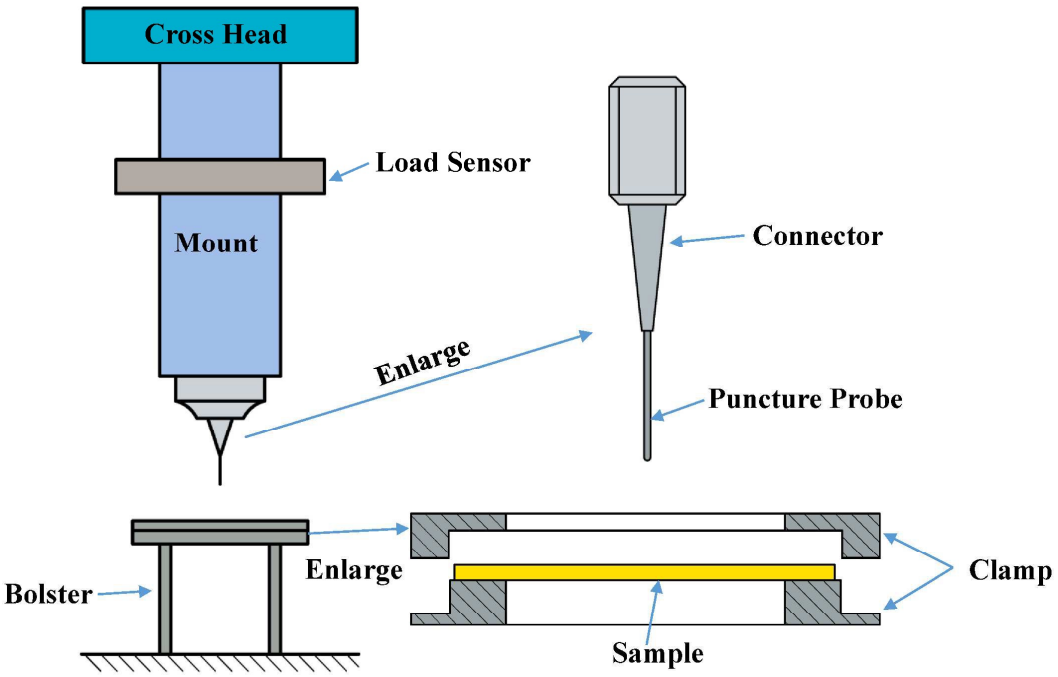

Fig. 1 Schematic of the puncture test setup.

2.5 Polarized optical microscope (POM)

POM (BX51, OLYMPUS, Japan) equipped with a video camera was used to observe the multilayered morphologies and to conduct puncture damage zone analysis of composites. For the layered morphology observation, an approximately 10-μm thin slice was obtained by a microtome along the extrusion direction. And for the damage zone analysis, the specimens were firstly cut through the damage zone center after puncture fracture, and then an approximately 15-μm thin slice was obtained by a microtome along the cross section surface for morphology observation.

2.6 Digital microscope analysis

The puncture fracture damage zones were imaged and analyzed from both the top view and the cross section view with a digital microscope (Keyence, VHX-1000C, Japan) at a magnification of 50. For the top view analysis, the samples after puncture were firstly fixed on the plasticine before observation. For the cross section view

analysis, the specimens were cut through the damage zone center and then flattened by a microtome.

3. Results and discussion

3.1 Phase morphology

Fig. 2 shows the POM micrographs of the multilayered HPP/POE morphologies with three extruder screw speed ratios (6:4, 7:3 and 8:2) of HPP and POE. The dark layer belonged to the POE, which had a low crystallinity, while the bright layer belonged to the HPP, which had a high crystallinity and exhibited a common spherulitic structure. Obviously all specimens had a laminar morphology, where the HPP and POE layers were aligned alternately. With greater than two layers, the layer thickness deviated slightly from the estimated value, *i.e.* the layers became thinner or thicker. This deviation was because the continuity and uniformity of the layers were strongly dependent on the viscosity ratio and interfacial instabilities of the components during coextrusion [24-26]. And the melt viscosity of the HPP was not the same as that of the POE. However, the viscosity difference between the two materials was so small that the layer continuity was relatively constant.

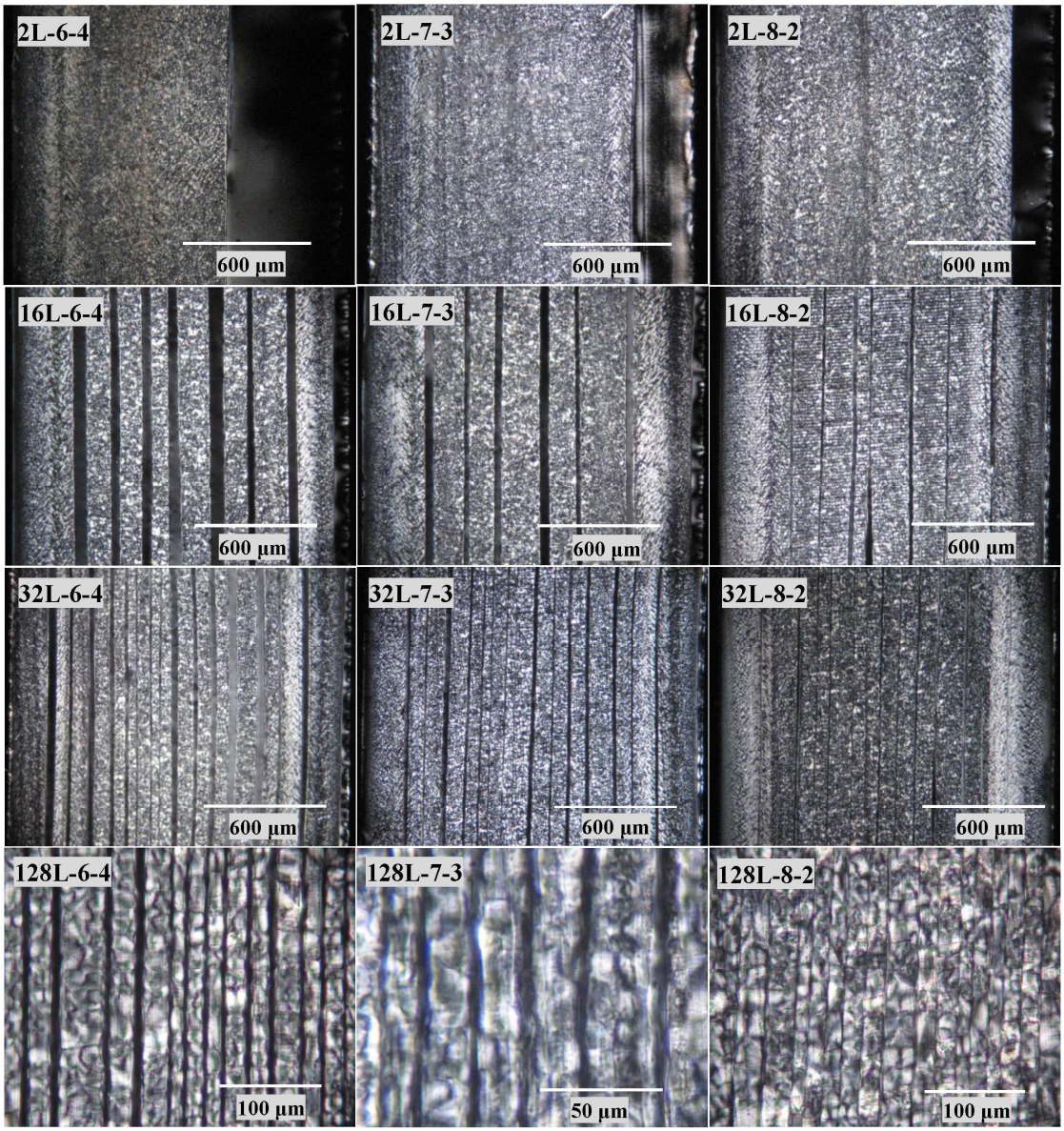

Fig. 2 Polarized optical micrographs of HPP/POE multilayered composites.

3.2 Puncture behaviors

The effect of phase structure on the puncture properties were studied with a puncture test. Fig. 3 shows the puncture load-displacement curves of HPP, multilayered and conventional composites with an extruder screw speed ratio of 8:2 and a probe tip diameter of 2 mm. It was found that all samples exhibited ductile failure with plastic deformation. The test temperature (23˚C) was above the glass-transition temperature

(T_g), hence the mobility of polymer chain could allow the samples to have plastic deformation before the occurrence of fracture [27]. Similar to the puncture of fiber-reinforced composites [28, 29], three regions could be identified on the load-displacement curves: the elastic region, the plastic region, and the fracture region. In the elastic region, the load increased quickly with slight increase of the displacement. And the deformation was elastic and could recover completely with the load removed. However, in the plastic region, the irreversible plastic deformation could occur. Further depression of the puncture tip into the specimen caused the distal surface to start cracking from tensile stress with fracture propagating through the whole sample thickness. This region was designated as the fracture propagation region. With the addition of POE, the slope of the load-displacement curve in the elastic region decreased, indicating a lower elastic modulus of puncture [1, 30]. Moreover, the puncture strength, which was obtained by the maximum load, also decreased with the addition of POE. The puncture strengths of the multilayered structure samples were higher than that of the conventional blend with the same volume fraction of POE. The load during the ductile puncture process was related to the stiffness of material. Hence the addition of elastomer POE could decrease the stiffness of HPP. However, it should be noted that the load of multilayered sample was higher than that of the conventional blend at the same displacement, indicating a high stiffness which was associated to the phase continuity of multilayered structure. In addition, compared with the instant rupture behaviors of the neat HPP and blend sample, the ruptures of multilayered structure samples took place in type of step by step. That was to say the different layers did not break simultaneously, as indicated by the drop stage in load.

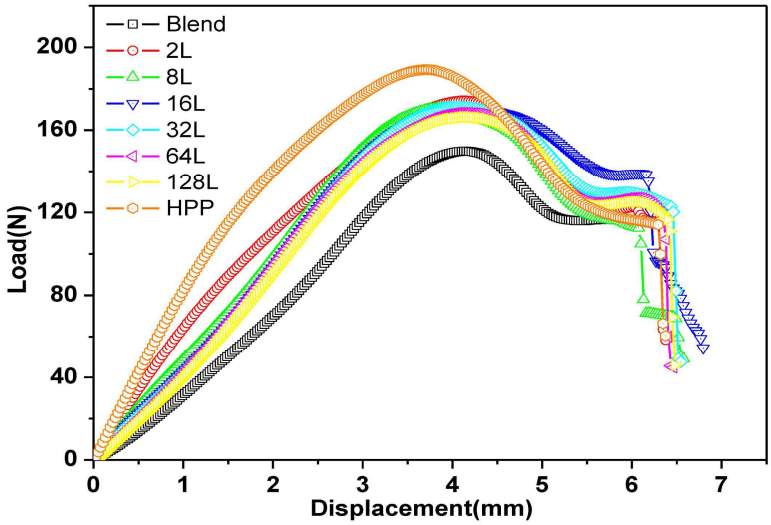

Fig. 3 The load-displacement curves of puncture for blend and multilayered specimens.

The puncture strengths of all samples with three different probes at the diameters of 1, 2 and 4 mm are shown in Fig. 4. The puncture strengths of multilayered samples were obviously higher than that of blend sample, which was consistent with the puncture load-displacement curves. Due to best phase continuity of multilayered structure, the mechanical properties, including the modulus, yield strength, and tensile strength, of multilayered structure are higher than those of conventional structure.[31-33] Consequently, the puncture strength, which seriously depends on the modulus, yield strength, and tensile strength, for multilayered structure were higher than that for blend sample.[27] And the puncture strengths of multilayered and blend samples were both decreased with the volume fraction of POE increasing, indicating a lower deformation resistance of puncture. This was due to the fact that the elastic POE could decrease the stiffness of HPP. Additionally, with the probes tip diameter increasing, the transverse tensile stress subjected in the interior of materials could become more dispersive. Therefore, to achieve the same strain, the larger external load was needed. Then the puncture strength would increase.[34] On the other hand, for the multilayered samples at a probe diameter of

1 mm, the 2-layer sample had relatively high puncture strength, due to all samples were perforated from the HPP layer to the POE layer. The rigid HPP layer was thicker than POE layer in 2-layer sample. Hence the puncture by a probe diameter of 1 mm was shown to proceed gradually as the probe perforated the sheet. Then the puncture resistance was mainly controlled by the rigid HPP layer, thus the 2-layer sample had relatively high puncture strength. Furthermore, with the probe diameter increasing, the failure mode would change from perforation gradually to perforation with more deformation around the probe tip [35]. Then the phenomenon that the 2-layer sample had relatively high puncture strength would disappear, as shown in Fig. 4b and 4c. In addition, for the multilayered samples with the same volume fraction of POE and probe diameter, a slight decrease trend of puncture strength with the layer number was observed. The interfaces between HPP and POE layers, where the chains of HPP and POE were tangled each other, could be treated as the conventional blend component. With increasing number of layers of multilayered composites, the content of interfaces increased, causing the proportion of blend component increased.[16] Therefore, the puncture strength of multilayered samples would slightly decrease with the number of layers increasing.

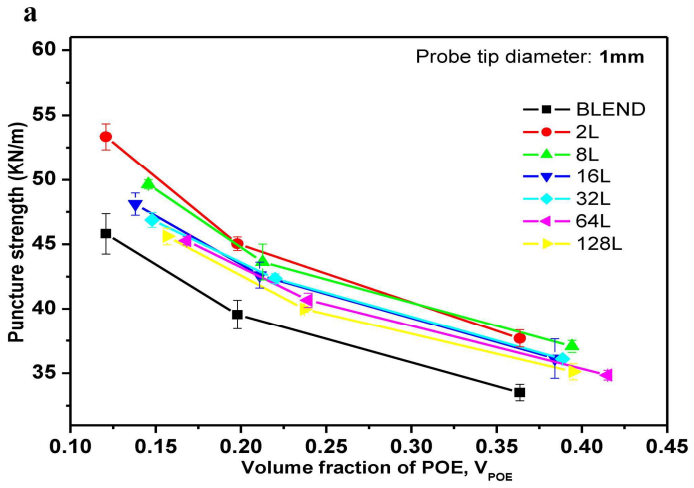

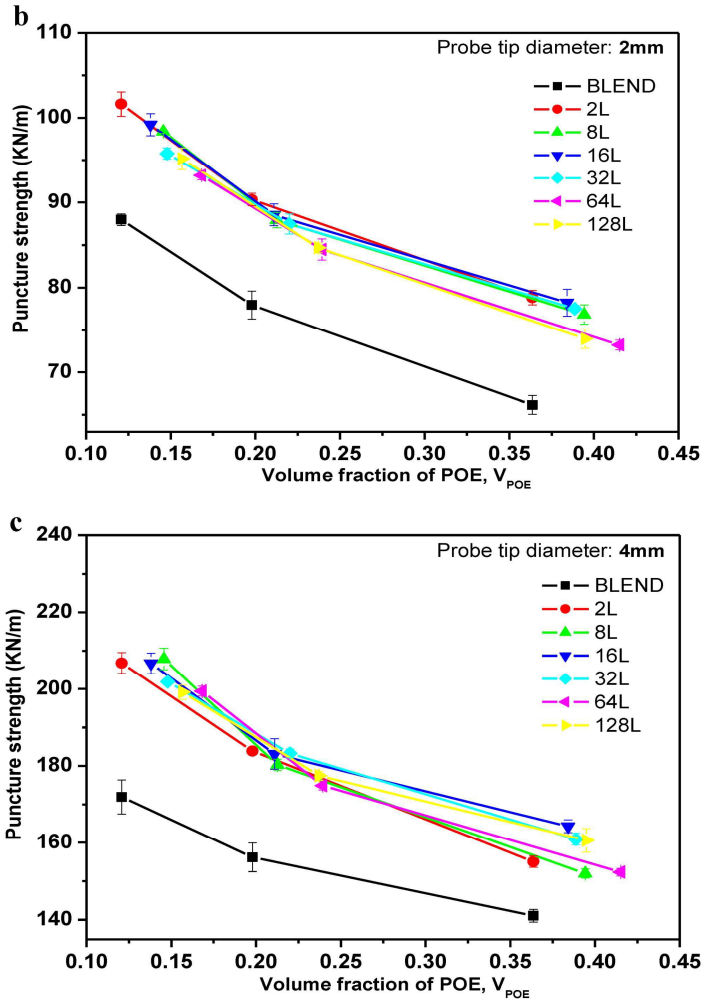

Fig. 4 The effects of volume fractions of POE and probe tip diameter on the puncture strength of multilayered and blend specimens.

Fig. 5 depicts the puncture energy according to the puncture load-displacement curves. The puncture resistance is typically expressed either as the puncture maximum load (puncture strength) or as the energy, *i.e.* the area under the load-deformation curve up to the point of puncture (puncture energy) [36]. And the puncture energy was found more sufficient to express the resistance to puncture. From Fig. 5, the trend of puncture energy with the volume fraction of POE, probe diameter, and number of layers, was found similar to that of puncture strength, due to the fact that the load-displacement curve which possessed a high load could have a large integrated area. Nevertheless, an

unusual phenomenon was found for the relative high puncture energy of 8-, 16- and 32-layer samples. Through inspecting the multilayered specimens at various stages of perforation, the interfacial delamination behavior caused by the deflection of crack when propagating perpendicular to the interface was confirmed. The interfacial delamination could consume some more puncture energy, and the instant rupture behaviors were delayed by crack deflection, expressed as the drop stage in load shown in Fig. 3. Hence the large increase in delamination area usually implied a large increase in energy absorption [28].

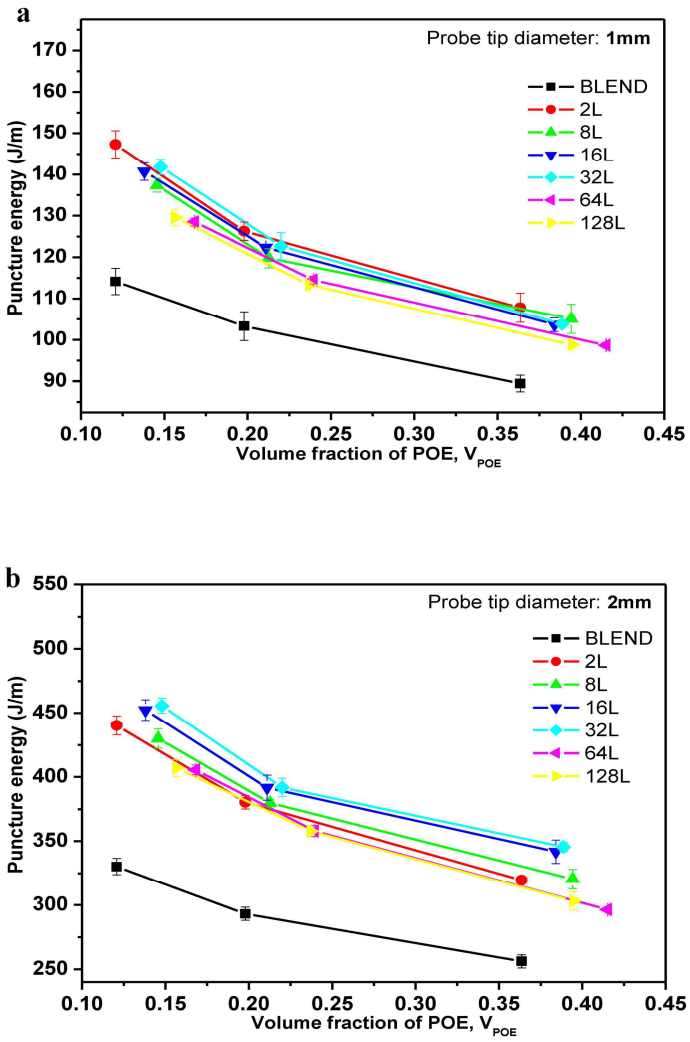

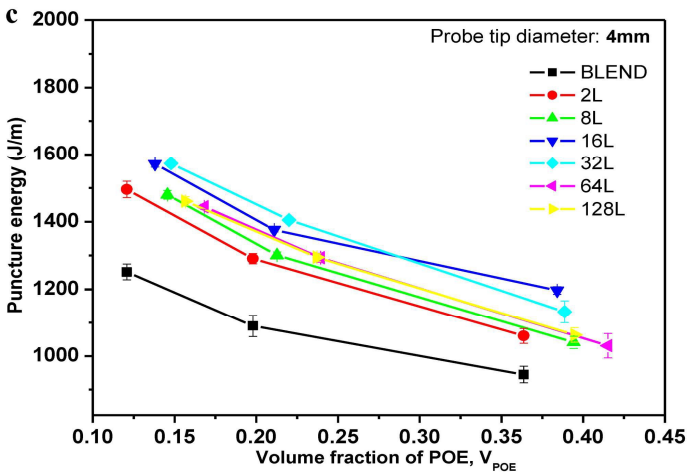

Fig. 5 The effects of volume fractions of POE and probe tip diameter on the puncture energy of multilayered and blend specimens.

3.3 Puncture Mechanism

The fracture damage zones of the top and cross section views of the bend samples with an extruder screw speed ratio of 8:2 are shown in Fig. 6. As a semi-crystalline polymer is deformed, its degree of crystallinity often increases, which in turn influences the transparency. This means that the stress state in the material can be followed by visually observing it as it is deformed [17]. Fig. 6a shows the images with the probe tip diameter of 1 mm, where a large plastic deformation occurred around the probe contact area. The top-view image showed that the blend sheet ruptured by a ductile hole enlargement type fracture with the material ahead of the puncture tip bulging out from the distal surface and conforming to the shape of the probe tip. The fracture occurred from the distal surface and was enlarged to the size of the probe tip. The cross-sectional view of the damage zone exhibited a large degree of sheet stretching, with material bulging out on the distal surface [37]. In addition, the whitening of the damage zone was observed, which was attributed to microvoid formation from bending deformation [38].

And the whitened area extended up to a distance of about seven times the probe diameter, indicating that the plastic deformation took place over a much larger area. A similar result was found in the Fig. 6b for the images with the probe tip diameter of 2 mm, and a center through-hole was also observed in the top view of the damage zone. The large plastic deformation occurred both in the probe contact area and the area far away from the probe. From the cross-sectional view, the rupture was observed to occur at the periphery of the probe. However, the stretching deformation was observed to increase with the probe diameter increasing. Therefore, the fracture mechanism of blend sample could be summarized as the sudden rupture when the stretching at the probe tip reached the failure value.

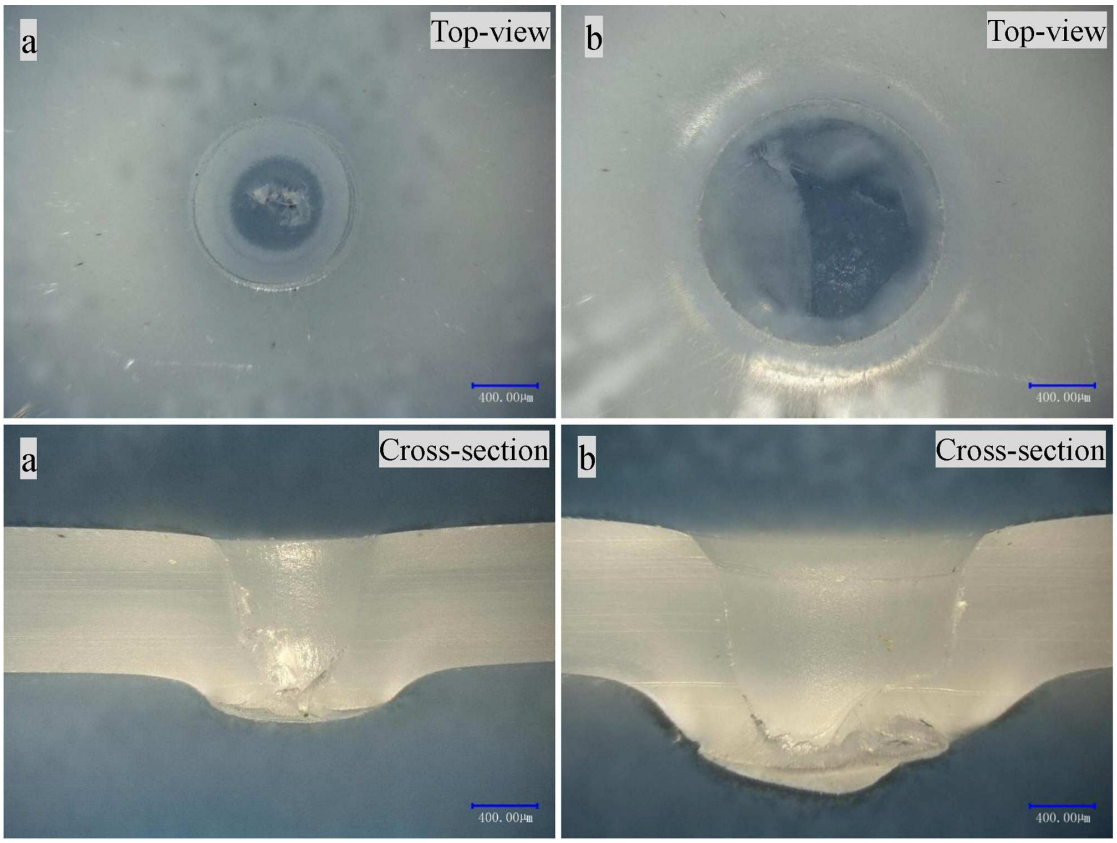

Fig. 6 The puncture fracture damage zones of the blend sample: (a) the probe tip diameter is 1 mm; (b) the probe tip diameter is 2 mm.

Fig. 7 shows the damage zones of the 16-layer sample with an extruder screw speed

ratio of 7:3. The top-view image of the damage zone also exhibited a center through-hole which conformed to the shape of the probe tip. The large plastic deformation occurred both in the probe contact area and the area far away from the probe. This type of damage zone was very similar to that of the blend sample. However, the cross-sectional view of the damage zone revealed a different puncture behavior. The individual layer might deform independently of each other during the perforation process. Puncture was shown to proceed gradually as the probe invaded the sheet. Meanwhile, the crack could deflect when propagating perpendicular to the interface and caused the interfacial delamination. Then, the different layers did not break simultaneously. The layer which was near the probe tip would firstly fracture. The ruptures of multilayered structure samples took place in type of step by step, which agreed well with the load-displacement curves. A closer inspection showed that both delamination and ductile tearing occurred within the individual layers. It could be concluded that the plastic deforming independently, interfacial delamination and ductile tearing of the layers were the main puncture failure mechanisms [37].

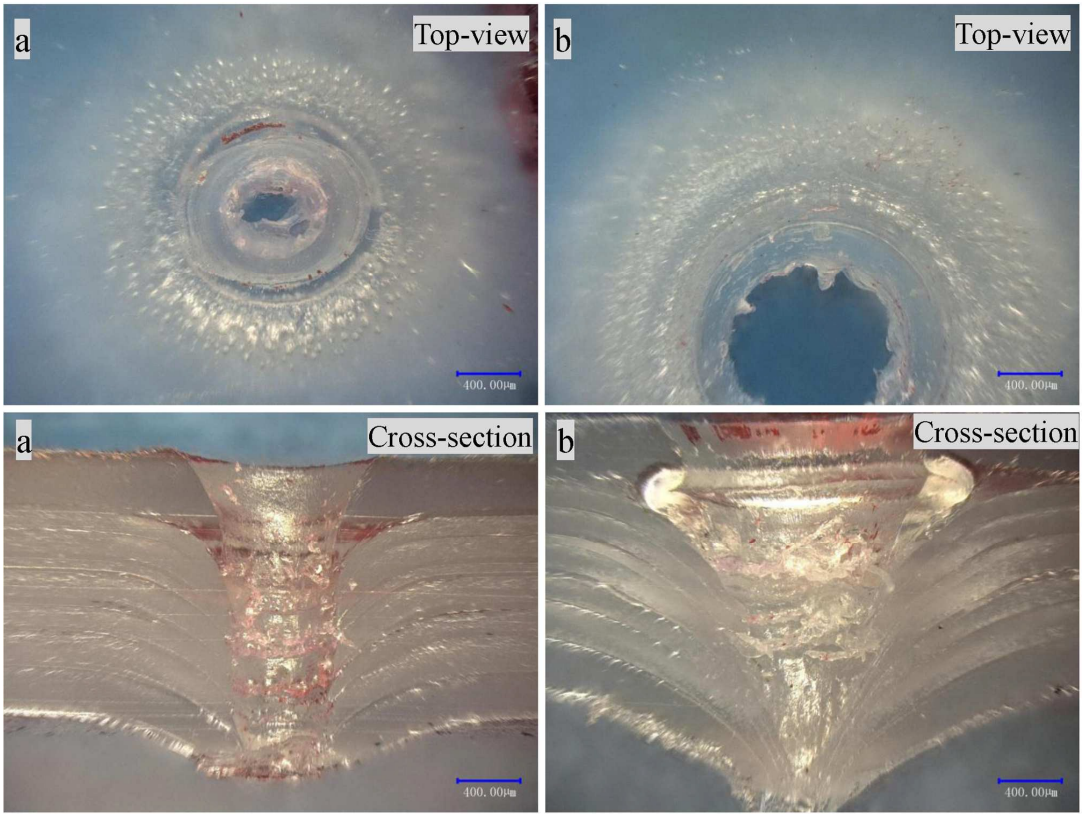

Fig. 7 The puncture fracture damage zones of the 16-layer sample: (a) the probe tip diameter is 1 mm; (b) the probe tip diameter is 2 mm.

To more directly observe the plastic deformation and fracture morphologies, an approximately 15-μm thin slice was obtained by a microtome along the cross section surface of the puncture sample. Then the polarized optical microscope was used for morphology observation. The POM images of the blend sample slices are shown in Fig. 8. The cross-sectional views of the damage zone exhibited a large degree of sheet plastic deformation before the final failure. The rupture occurred suddenly when the strain at the probe tip reaches the failure value. Essentially, the local perforation was controlled by a mixture of tensile and shear stresses around the probe tip. In addition, the amount of sheet stretching deformation increased with the probe diameter increasing, indicating an increased ductility. This was due to the stress concentration around the probe when perforating decreased with the probe diameter increasing.

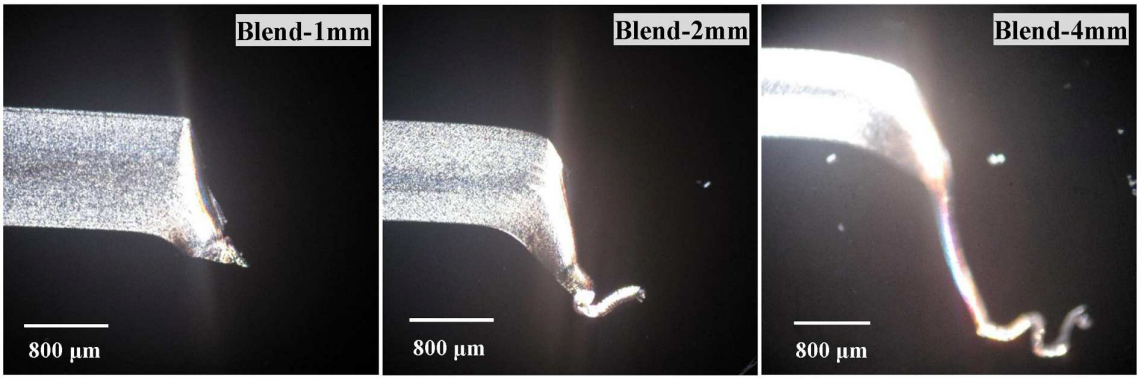

Fig. 8 The POM images of the blend sample slices obtained from the puncture damage zone.

Fig. 9 depicts the POM images of the multilayered sample slices. Here the perforation behavior could be directly observed. The cross-sectional views of the damage zones exhibited a large degree of sheet plastic deformation before the final tear failure, which was very similar to that of blend samples. Whereas the puncture ruptures of multilayered structure samples took place in type of step by step. The individual layer deformed and perforated independently of each other during the puncture process. Furthermore, it should be noted that the obvious interfacial delamination failure was confirmed. As discussed above, the delamination was caused by crack propagation deflection. And it was controlled by a mixture of the transverse tensile and shear stresses existed in the HPP and POE layers [28] . When the differences of tensile and shear stresses between the adjacent layers during the puncture perforation exceeded the stress that crack initiation needed, the crack at the interface would be initiated and propagated, causing the origination of interlayer peeling. Then the deformation energy would be dissipated by the multiple crack arrest and initiation at the interface.[39] As a result, some load drop stages appeared in the load-displacement curve, as indicated in Fig. 3. Then the sudden rupture when the stretching at the probe tip reached the failure value could develop into the staged rupture behavior. Therefore, the multilayered samples, in which

the delamination occurred, could absorb considerably more energy up to fracture (*i.e.*, a larger area under the load-displacement curve). And the puncture resistance was enhanced by the primary energy absorbing mechanisms, *i.e.* the plastic deforming independently, interfacial delamination and ductile tearing of the layers.

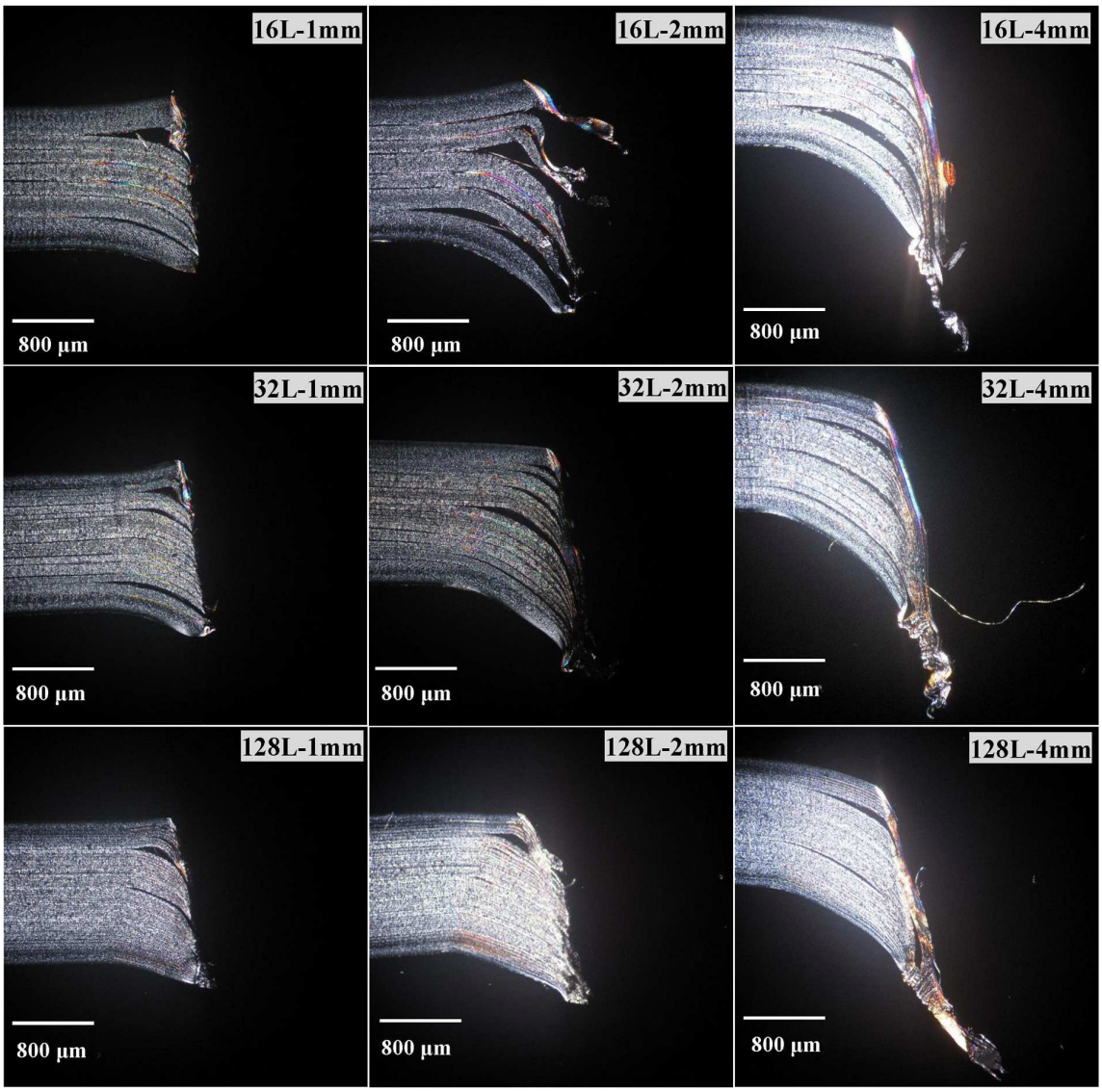

Fig. 9 The POM images of the multilayered sample slices obtained from the puncture damage zone.

4. Conclusions

The multilayered structure polymer sheets were successfully fabricated through the multilayered coextrusion system designed in our lab. The effects of the phase structure,

the layer number, the volume fraction of POE and the probe size on the puncture resistance were studied in detail. The puncture strength and energy of multilayered and blend samples were both decreased with the volume fraction of POE increasing, due to the decrease of the stiffness. And the puncture strength and energy could both increase with the probe tip diameter increasing. More importantly, it was found that the puncture behavior depended strongly on the phase structure. The puncture strength and energy of the multilayered sheets were higher than those of the conventional blend, which correlated with the best phase continuity of multilayered structure. Compared with the sudden rupture behavior of the blend when the deformation at the probe tip reached the failure value, the puncture mechanisms of multilayered samples were more complex. Due to the tensile and shear stresses differences between the adjacent layers during the puncture perforation, the obvious interfacial delamination failure was confirmed. The puncture of multilayered samples could develop into the staged rupture behavior. Therefore, the puncture resistance was enhanced by the primary energy absorbing mechanisms including the plastic deforming independently, interfacial delamination and ductile tearing of the layers.

Acknowledgments

The authors are grateful to the National Natural Science Foundation of China (51227802, 50933004, 51073099 and 51121001), the Ministry of Education Priority Funding Areas (20110181130004), and the Program for New Century Excellent Talents in University （NCET-10-0593) for financial support of this work.

References

1. O. N. Scott, M. R. Begley, U. Komaragiri and T. J. Mackin, *Acta Mater*, 2004, 52, 4877-4885.

2. H. Daiyan, E. Andreassen, F. Grytten, O. V. Lyngstad, T. Luksepp and H. Osnes, *Polym Test*, 2010, 29, 648-657.

3. C. T. Nguyen, T. Vu-Khanh and J. Lara, *Theor Appl Fract Mec*, 2004, 42, 25-33.

4. L. F. Leslie, J. A. Woods, J. G. Thacker, R. F. Morgan, W. McGregor and R. F. Edlich, *J Biomed Mater Res*, 1996, 33, 41-46.

5. L. M. Carapellucci, A. F. Yee and R. P. Nimmer, *Polym Eng Sci*, 1987, 27, 773-780.

6. R. Wilson-Fahmy, D. Narejo and R. Koerner, *Geosynth Int*, 1996, 3, 605-628.

7. D. Narejo, R. Koerner and R. Wilson-Fahmy, *Geosynth Int*, 1996, 3, 629-653.

8. C. Nguyen and T. Vu-Khanh, *J Mater Sci*, 2004, 39, 7361-7364.

9. C. Nguyen, T. Vu-Khanh, P. Dolez and J. Lara, *Int J Fracture*, 2009, 155, 83-91.

10. J. Wang, C. Wang, X. Zhang, H. Wu and S. Guo, *RSC Adv*, 2014, 4, 20297-20307.

11. F. Ania, F. J. Baltá-Calleja, A. Flores, G. H. Michler, S. Scholtyssek, D. Khariwala, A. Hiltner, E. Baer, L. Rong and B. S. Hsiao, *Eur Polym J*, 2012, 48, 86-96.

12. G. He, J. Li, F. Zhang, F. Lei and S. Guo, *Polymer*, 2014, 55, 1583-1592.

13. J. Kerns, A. Hsieh, A. Hiltner and E. Baer, *J Appl Polym Sci*, 2000, 77, 1545-1557.

14. D. Haderski, K. Sung, J. Im, A. Hiltner and E. Baer, *J Appl Polym Sci*, 1994, 52, 121-133.

15. E. Baer, A. Hiltner and H. Keith, *Science*, 1987, 235, 1015-1022.

16. J. Shen, M. Wang, J. Li, S. Guo, S. Xu, Y. Zhang, T. Li and M. Wen, *Eur Polym J*, 2009, 45, 3269-3281.

17. J. Lange, H. Mokdad and Y. Wysery, *J plast film sheet*, 2002, 18, 231-244.

18. J. Shen, M. F. Champagne, R. Gendron and S. Guo, *Eur Polym J*, 2012.

19. S. Yang, H. Yu, F. Lei, J. Li, S. Guo, H. Wu, J. Shen, Y. Xiong and R. Chen, *Macromolecules*, 2015, 48, 3965-3973.

20. F. Zhang, G. He, K. Xu, H. Wu and S. Guo, *RSC Adv*, 2014, 4, 20620-20625.

21. J. Shen, J. Li and S. Guo, *Polymer*, 2012, 53, 2519-2523.

22. S. Das, S. Laha and A. Ghatak, *Soft Matter*, 2014, 10, 6059-6067.

23. S. Das and A. Ghatak, *J Mater Sci*, 2011, 46, 2895-2904.

24. H. Wang, J. K. Keum, A. Hiltner, E. Baer, B. Freeman, A. Rozanski and A. Galeski, *Science*, 2009, 323, 757-760.

25. J. Luo, Y. Liang, J. Yang, H. Niu, J. Y. Dong and C. C. Han, *Polymer*, 2011, 52, 4590-4599.

26. M. Gupta, Y. Lin, T. Deans, E. Baer, A. Hiltner and D. A. Schiraldi, *Macromolecules*, 2010, 43, 4230-4239.

27. Y. Yang, M. Ponting, G. Thompson, A. Hiltner and E. Baer, *J Appl Polym Sci*, 2012, 124, 2524-2536.

28. R. A. W. Mines, A. M. Roach and N. Jones, *Int J Impact Eng*, 1999, 22, 561-588.

29. J. N. Baucom and M. A. Zikry, *Compos Part A Appl S*, 2005, 36, 658-664.

30. W. Yang and K. Hsu, *J Appl Mech*, 1971, 38, 227-230.

31. J. Gámez-Pérez, O. O. Santana, A. Gordillo and M. L. Maspoch, *Polym Eng Sci*, 2007, 47, 1365-1372.

32. G. He, F. Zhang, L. Huang, J. Li and S. Guo, *J Appl Polym Sci*, 2014, 131, 7545-7553.

33. J. Kolark, *Eur Polym J*, 1998, 34, 585-590.

34. S. Fakhouri, S. B. Hutchens and A. J. Crosby, *Soft Matter*, 2015, 11, 4723-4730.

35. C. Nguyen, T. Vu-Khanh, P. Dolez and J. Lara, *Int J Fracture*, 2009, 155, 75-81.

36. R. J. Seyler, *J plast film sheet*, 1990, 6, 191-224.

37. M. R. Abdullah and W. J. Cantwell, *Compos Sci Technol*, 2006, 66, 1682-1693.

38. Y. Liu and R. W. Truss, *J Polym Sci Pol Phys*, 1994, 32, 2037-2047.

39. A. Ghatak, L. Mahadevan, J. Y. Chung, M. K. Chaudhury and V. Shenoy, *Proc Roy Soc Lond Ser A*, 2004, 460, 2725-2735.

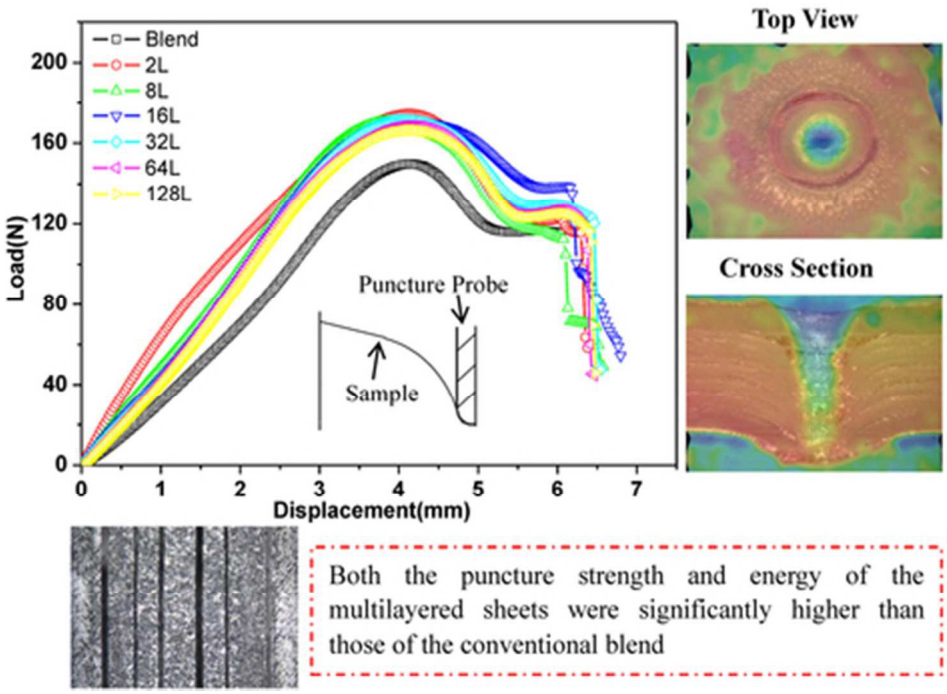

39x29mm (300 x 300 DPI)